Automatic parameter setting for balloon models

Jörg Bredno, Thomas Lehmann, Klaus Spitzer
Institute of Medical Informatics, Medical Faculty
Aachen University of Technology (RWTH), D–52057 Aachen, Germany

ABSTRACT

We describe a "learning–from–examples"–method to automatically adjust parameters for a balloon model. Our goal is to segment arbitrarily shaped objects in medical images with as little human interaction as possible. For our model, we identified six significant parameters that are adjusted with respect to certain applications. These parameters are computed from one manual segmentation drawn by a physician. (1) The maximal edge length is derived from a polygon–approximation of the manual segmentation. (2) The size of the image subset that exerts external influences on edges is set according to the scale of gradients normal to the contour. (3) The offset of the assignment from greylevels to image potentials is adjusted such that the propulsive pressure overcomes image potentials in homogeneous parts of the image. (4) The gain of this assignment is tuned to stop the contour at the border of objects of interest. (5) The strength of deformation force is computed to balance the contour at edges with ambiguous image information. (6) These parameters are computed for both, positive and negative pressure. The variation that gives the best segmentation result is chosen. The analytically derived adjustments are optimized with a genetic algorithm that evolutionarily reduces the number of misdetected pixels. The method is used on a series of histochemically stained cells. Similar segmentation quality is obtained applying both, manual and automatic parameter setting. We further use the method on laryngoscopic color image sequences, where, even for experts, the manual adjustment of parameters is not applicable.

Keywords: active contour, balloon model, parameter adjustment, learning from examples, genetic algorithm, image segmentation, color segmentation

1. INTRODUCTION

Active contour models are widely used for segmentation of medical images.[1] Balloon models allow the detection of any desired shape but require specific adaptation of parameters, such as influences and their weights, for each segmentation task.[2] So far, this parameter setting requires expert knowledge and time–consuming manual interaction,[3] which physicians can't perform. Hence, these models are not routinely used in medicine.

In this paper, strategies for automatic parameter setting are introduced which allow physicians to use these models. Our method of "learning–from–examples" combines an analysis of the influences that act on the model[4] with a genetic algorithm that optimizes the agreement of a current with a manual reference segmentation.[5] Such methods usually are bounded to greylevel images.[3] Furthermore, many published methods only are used to segment images from an image stack with propagation methods. They are not applicable on images where no initial contour is present. For those tasks, balloon models offer significant advantages.[6] We introduce methods for the automatic parameter setting to segment medical images where no initial contour and shape knowledge exists, and, furthermore, for color and other multi–channel images where manual parameter settings are impossible.

2. THE DEFORMABLE MEMBRANE BALLOON MODEL

The parameters automatically are set for a simplified two–dimensional instance of a general finite element model[7] that has been used for a wide variety of different quantification tasks in medical image analysis.[8]

Our model represents shapes as polygons formed by N vertices v_i and N straight edges e_j which connect two vertices v_j and v_{j+1}. Each vertex defines a position $\vec{v}_i$ in the image space $I \subset \mathbb{N}_0^2$ and supports two edges e_{i-1} and

Further author information: Send correspondence to Jörg Bredno
Institute of Medical Informatics, Aachen University of Technology (RWTH), D–52057 Aachen, Germany
E–mail: jbredno@mi.rwth-aachen.de

In *Medical Imaging 2000: Image Processing*, Kenneth M. Hanson, Editor,
Proceedings of SPIE Vol. 3979 (2000) • 1605-7422/00/$15.00

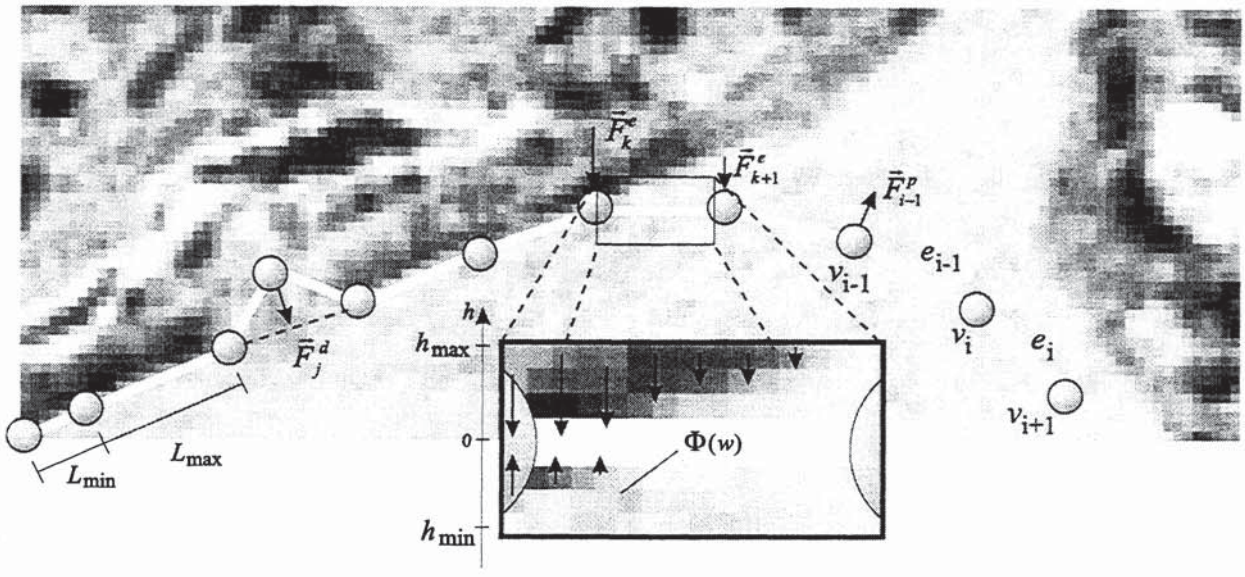

Figure 1. Mechanical influences during a segmentation process.

e_i. The contour is circular. For all following notations we assume that $v_{N+i} = v_i, e_{N+i} = e_i$. The image itself is interpreted as an assignment $\vec{f} : \vec{x} \in I \rightarrow \vec{w} \in W$ that maps the image space I onto the value space $W \subset \mathbb{R}^m$. The model is not limited to greylevel images ($m = 1$). The automatic parameter setting is needed more intensely for color images ($m = 3$). Mechanical influences are calculated for the edges and vertices of the model and drive an iterative segmentation process. For their computation, the length of edges $|e_j|$ and their unity normal vector $\vec{n}_j$ pointing outward are used.

In our model, the contour is influenced by an internal or external pressure p. This influence defines the seeking tendency of all balloon models as far as not in contact with significant image information. It results in a pressure force $\vec{F}^p_i$ that is transferred from the edges e_{i-1} and e_i onto the vertex v_i:

$$\vec{F}^p_i = \frac{p}{2}(|e_{i-1}| \cdot \vec{n}_{i-1} + |e_i| \cdot \vec{n}_i) \tag{1}$$

Internal influences aim to reduce the model's 2^{nd} order derivative. We use a simple method for the deformation forces $\vec{F}^d_i$. Every vertex v_i is pulled with adjustable strength s_d to the center of its surrounding vertices v_{i-1} and v_{i+1}.

$$\vec{F}^d_i = s_d \cdot \left(\frac{\vec{v}_{i+1} + \vec{v}_{i-1}}{2} - \vec{v}_i \right) \tag{2}$$

Image information is read in rectangular areas around edges. We define image potentials $\vec{\Phi}(\vec{w})$ that are mapped onto the value space. These image potentials define the strength of external influences. If the dimension of the value space is $m = 1$, then Φ is a scalar assigned to the image's greylevels w. For value spaces of higher dimension, we use an individual mapping of the components of $\vec{w}$ to the components of $\vec{\Phi}$. A filter kernel $\vec{k}(h)$ reflects the appearance, strength, and scale of gradients in different components of the image values. The force resulting from external influences is an unstandardized correlation of image potentials and the filter kernel. It is computed by summing all image potentials $\vec{\Phi}(\vec{f}(\vec{x}))$ in the rectangular area around edges bounded by h_{min} and h_{max}. The image potentials are multiplied with the kernel filter $\vec{k}(h)$ in dependency of the distance h to the edge (Fig. 1):

$$\vec{F}_i^e = -\vec{n}_i \sum_{\lambda=0}^{|e_i|} \sum_{h=h_{\min}}^{h_{\max}} \vec{k}(h) \cdot \vec{\Phi}\left(\vec{f}\left(\vec{v}_i + \frac{\lambda}{|e_i|}(\vec{v}_{i+1} - \vec{v}_i) + h \cdot \vec{n}_i\right)\right) \cdot \frac{\lambda}{|e_i|}$$
$$-\vec{n}_{i-1} \sum_{\lambda=0}^{|e_{i-1}|} \sum_{h=h_{\min}}^{h_{\max}} \vec{k}(h) \cdot \vec{\Phi}\left(\vec{f}\left(\vec{v}_i + \frac{\lambda}{|e_{i-1}|}(\vec{v}_{i-1} - \vec{v}_i) + h \cdot \vec{n}_{i-1}\right)\right) \cdot \frac{\lambda}{|e_{i-1}|} \quad (3)$$

Even though many other interpolation methods are known,[9] we use nearest neighbor interpolation so far to map continuous positions $\vec{x}$ into the discrete image space I. The computation of the external force $\vec{F}_i^e$ in Eq. 3 respects the equilibrium of turning moments of external influences.[8]

A segmentation process with the balloon model is initialized either as a small circular structure to be inflated or as a rectangle that surrounds the entire image for deflation. Then, the forces are computed and lead to an iterative movement of vertices. For this movement, $\vec{F}_i^p$ and $\vec{F}_i^e$ are normalized with respect to the size of adjacent edges.

$$\Delta\vec{v}_i = \frac{1}{\beta}\left(\vec{F}_i^d + \frac{2}{|e_i| + |e_{i-1}|}(\vec{F}_i^p + \vec{F}_i^e)\right) \quad (4)$$

Here, β denotes the coefficient of liquid friction, where the velocity of objects is proportional to imposed forces. After each iteration, the contour is resampled so that the size of edges lays within a defined range $[L_{\min}, L_{\max}]$. An intersection of edges may occur due to the free movement of vertices. These inconsistencies are solved by deleting the inverse part of the intersected contour.[4,10] The iteration converges when the vertices have reached a stable state where no significant movement occurs.

3. ADJUSTMENT OF PARAMETERS FROM MANUAL SEGMENTATION

Our model is able to detect the contour of objects in images if its controlling parameters are adjusted to the image material and the appearance of interesting objects. For a specific segmentation task, the following parameters must be adjusted:

- The sampling of the contour defined by the minimal and maximal edge lengths $L_{\min}$ and $L_{\max}$.
- The scale of gradients which is reflected by $h_{\min}$ and $h_{\max}$.
- The appearance and intensity of gradients which are reflected by $\vec{k}(h)$.
- The mapping $\vec{\Phi}\left(\vec{f}(\vec{x})\right)$ of image values to image potentials.
- The strength s_d of the deformation force.
- The sign of the pressure p.

No precise grammar exists that allows users to describe the appearance of objects of interest. If a segmentation is needed for an automated quantification of a series of images, the physician draws a manual segmentation result for one exemplary image. Here, any image manipulation software can be used. Then, the parameters are adjusted automatically to result in a precise segmentation for this initial image. The obtained parameter set is used for all other images in the series.

3.1. Sampling of the Contour

First, we create a simple polygon–approximation of the manual segmentation. We start at the center of gravity of the manual segmentation and cast rays from this center into 20 directions with a difference angle of $\frac{\pi}{20}$. We determine the part of these rays that lays completely inside the segmented object. The longest of these rays is used to define an initial contour that consists of only two vertices at the border of the object and two connecting edges for the following polygon–approximation. If the center of gravity does not lay inside the segmented object, we also use the casting of rays to find a point inside the object near to the center.

With this initial contour, an iterative algorithm is started:

- For each edge, we search for the corresponding pixel on the border of the object with the largest Cartesian distance to the edge. If this value is above a predefined maximal distance Δ,[11] a new vertex is placed at this position.
- If the maximal distance is below Δ, the edge is disregarded.
- Else, the edge is broken up into two edges that are supported by the new vertex. Both new edges are processed in the same way as the originating edge.
- The algorithm terminates if no more pixel on the border of the manual segmentation is found that lays more than Δ apart of an edge.

The computation of the maximal distance is initiated at every pixel that belongs to the edge. If this pixel lays within the segmented object, the transition to the outside is searched right angled to the edge starting at this position. Otherwise, the search is performed to the inside. The search towards the outside of the object is allowed only if at least one line from the current pixel to the vertices of the current edge does not cut the border of the segmented object.

The resulting polygon–approximation has uneven edge lengths $|e_i|$. We use this contour to set $L_{\min}$ and $L_{\max}$:

$$L_{\max} = \xi_{0.05}\left(\sqrt{(\vec{v}_i - \vec{v}_{i+2})^2},\, i \in [0,\ldots,N-1]\right),\; L_{\min} = \frac{2}{5}L_{\max} \tag{5}$$

The maximum edge length $L_{\max}$ is set to the 5%–quantile of the Cartesian distances between vertices that lay two edges apart because an edge of this length would have to be splitted during the segmentation process. $L_{\min} = \frac{2}{5}L_{\max}$ was chosen heuristically.

3.2. Scale and intensity of gradients

In the following sections, we suppose that the parameters are set for an inflating segmentation of an image with 256 greylevels. The extension to color or other multi–channel images as well as shrinking segmentations is derived from these methods. Furthermore, we assume that the inside of the segmented object in average is darker than the outside.

In order to determine the scale of the gradient across the border of the segmented object, which is reflected by $h_{\max}$ and $h_{\min}$, we compute histograms $H(d)$ for each image subset $I(d)$. These subsets contain all pixels that have the distance d to the polygon–approximated contour:

$$I(d) = \left\{ \vec{x} \in I \;\middle|\; \vec{x} = \vec{v}_i + \frac{\lambda}{|e_i|}(\vec{v}_{i+1} - \vec{v}_i) + d \cdot \vec{n}_i,\, \lambda \in [0,\ldots,|e_i|],\, i \in [0,\ldots,N-1] \right\} \tag{6}$$

$I(d)$ lays on the outside of the contour for $d > 0$ and on the inside for $d < 0$, respectively. The $H(d)$ are used to determine those image subsets $\bigcup I(d_i)$ on the inside and outside of the contour that could be distinguished best by threshold segmentation. The subsets $I(d_i)$ are combined in varying ranges of an inner and outer distance, d_1 and d_2, respectively. A threshold classification of the in– and outside of the contour would result in the classification error $E_c(d_1, d_2)$. To determine $E_c(d_1, d_2)$ that is achieved by using the combination d_1 and d_2, let $h(d, g)$ be the number of pixels in $I(d)$ with greylevel g, i.e. one entry in the histogram $H(d)$:

$$E_c(d_1,d_2) = \min_{t=0}^{255} \frac{\sum_{d=d_1}^{d_2} \left(\sum_{g=0}^{t-1} h(-d,g) + \sum_{g=t}^{255} h(d,g) \right)}{2 \cdot (d_2 - d_1 + 1) \cdot \sum_{i=0}^{N-1} |e_i|} \tag{7}$$

Assuming that the inside of the contour is darker than the outside, E_c gives the relative number of pixels that would have been misclassified if an optimal threshold segmentation would have been used in the vicinity of the object's border.

Different E_c are computed for all combinations of $1 \leq d_1 < d_2 \leq d_{\max}$ to find the optimal classification error $\widehat{E_c}$ and the optimal scale, which is denoted by $\widehat{d_1}$ and $\widehat{d_2}$. We use these values to define a representative subsets of pixels on the inside I_{in} and outside I_{out} of the contour:

$$I_{\text{in}} = \bigcup_{d=-\widehat{d_2}}^{-\widehat{d_1}} I(d), \qquad I_{\text{out}} = \bigcup_{d=\widehat{d_1}}^{\widehat{d_2}} I(d) \tag{8}$$

For these subsets, we compute μ_{in} and σ_{in} to describe statistically the greylevels of I_{in}, and μ_{out} and σ_{out} for I_{out} respectively. The values $\widehat{d_1}$, $\widehat{d_2}$, μ_{in}, σ_{in}, μ_{out}, and σ_{out} are used to define the the filter kernel $k(h)$ and the greylevel potentials $\Phi(w)$. At this point, it can not be distinguished between two different kinds of optimal parameter setting, both variations are computed and later compared by their segmentation result on the image itself.

3.2.1. Variation 1

In some cases, the in– and outside of the contour might have characteristic greylevels that can be used to distinguish between these regions. In this case, the balloon model detects the first coherent occurrence of greylevels that are supposed to belong to the outside of the contour. We simply set $h_{\min} = \widehat{d_1}$, $h_{\max} = \widehat{d_2}$, $k(h) = 1 \,\forall\, h \in [h_{\min}, h_{\max}]$. Furthermore, the potentials of greylevels are set with respect to the inner pressure that must overcome potentials inside the object. The contour is stopped from potentials on the outside of the manually segmented object. The resulting requirements

$$p > \sum_{h=h_{\min}}^{h_{\max}} k(h) \cdot \mu_{\text{in}} \qquad \wedge \qquad p < \sum_{h=h_{\min}}^{h_{\max}} k(h) \cdot \mu_{\text{out}} \tag{9}$$

can be solved by defining a plateau for all greylevels that are supposed to belong to the inside, and a linear gain for higher greylevels. The junction between these two segments is placed at the point w_0 that lays the same fraction α of σ_{in} and σ_{out} afar of μ_{in} and μ_{out}, respectively.

$$\begin{aligned} w_o &= \mu_{\text{in}} + \alpha\sigma_{\text{in}} \stackrel{!}{=} \mu_{\text{out}} - \alpha\sigma_{\text{out}} \\ \Rightarrow w_o &= \frac{\mu_{\text{in}} \cdot \sigma_{\text{out}} + \mu_{\text{out}} \cdot \sigma_{\text{in}}}{\sigma_{\text{in}} + \sigma_{\text{out}}}. \end{aligned} \tag{10}$$

The gain is computed so that the external force caused by greylevels μ_{out} is stronger than the influence of the internal pressure:

$$\Phi(w) = \begin{cases} \dfrac{S_p \cdot p}{(\mu_{\text{out}} - w_0)(\widehat{d_2} - \widehat{d_1} + 1)}(w - w_0) & \forall \quad w > w_0 \\ 0 & \text{else} \end{cases} \tag{11}$$

Here, S_p denotes a safety factor so that the contour is also stopped at parts of the object's boundary where the greylevel difference is less than the average $\mu_{\text{out}} - \mu_{\text{in}}$.

3.2.2. Variation 2

For other images, it is more promising if the active contour model is stopped by gradients in the image rather than the occurrence of greylevels. In these cases, we set

$$k(h) = \begin{cases} -1 & \forall \quad h \in [-\widehat{d_2}, -\widehat{d_1}] \\ 1 & \forall \quad h \in [\widehat{d_1}, \widehat{d_2}] \\ 0 & \text{else} \end{cases} \tag{12}$$

Here, the offset of the image potentials is irrelevant because the external force is zero for all homogenous image parts. The external force at the object's boundary should exceed the influence resulting from inner pressure. We set

$$\Phi(w) = \frac{S_p \cdot p}{(\widehat{d_2} - \widehat{d_1} + 1)(\mu_{\text{out}} - \mu_{\text{in}})} \cdot w. \tag{13}$$

Again, S_p is a safety factor that increases the strength of the external influences so that the contour is also stopped at weaker gradients around the object's border.

3.3. Deformation Force

The aim of the deformation force is to smooth the contour and to tight vertices to the contour that would cross an object's border in areas with ambiguous image information. To adjust the parameter s_d, the polygon–approximation is resampled to the determined $L_{\max}$ and $L_{\min}$. For the resulting contour, one single iteration step is performed that only bases on pressure and external influences. Then, for each vertex v_i, the sum of forces $\begin{pmatrix} F_x \\ F_y \end{pmatrix} := \vec{F}^e + \vec{F}^p$ and the deformation force $\begin{pmatrix} F_x^d \\ F_y^d \end{pmatrix} := \vec{F}^d$ are computed for $s_d = 1$. (The indices i are omitted for simplification reasons). The individual s_d that results in a minimal total of the sum of all forces is calculated for each vertex v_i:

$$\begin{aligned} \left| \begin{pmatrix} F_x \\ F_y \end{pmatrix} + s_d \begin{pmatrix} F_x^d \\ F_y^d \end{pmatrix} \right| &= \sqrt{(F_x + s_d \cdot F_x^d)^2 + (F_y + s_d \cdot F_x^y)^2} \stackrel{!}{=} \min \\ \Rightarrow s_d &= -\frac{F_x F_x^d + F_y F_y^d}{F_x^{d2} + F_y^{d2}} \end{aligned} \tag{14}$$

For the contour, we use the third quartile $\xi_{0.75}$ of all these individual s_d.

3.4. Selection of variations

All parameters are computed for both variations. Afterwards, two more parameter sets are determined to examine whether a shrinking segmentation with $p < 0$ leads to better results. Then, a segmentation process is started for all four parameter sets. For these segmentations, the number of erroneous pixels N_e, where the detected contour differs from the manual segmentation, are counted. Finally, the parameter set with the smallest N_e is chosen.

4. OPTIMIZATION BY GENETIC ALGORITHM

The analytic rules described so far do not reflect inhomogeneities which are inherent in medical data. A parameter set adjusted by the rules above may still produce segmentation errors even for the original image. Therefore, a genetic algorithm[12] is used to improve the parameter set. In this evolutionary optimization, the individuals are parameter sets with a fitness $1/N_e$. The genetic algorithm is started to find the highest possible fitness function within an evolving population. Each individual i in this population is a parameter set $P_i = \{\vec{p}_{i,j}\}$. The two–dimensional vector $\vec{p}_{i,j}$ consists of a parameter's value $\text{val}_{i,j}$ combined with its variability during reproduction $\text{var}_{i,j}$.

4.1. Initialization

The search space for the optimal fitness function consists of the maximal edge length $L_{\max}$, the gain and the transition point of the assignment $\Phi(w)$, and the strength s_d of the deformation force. The initial variability $\text{var}_{i,j}$ of all parameters is set to $\frac{1}{5}$ of their absolute initial value $\text{val}_{i,j}$. The genetic algorithm is initialized by only one individual ancestor that was computed as described above.

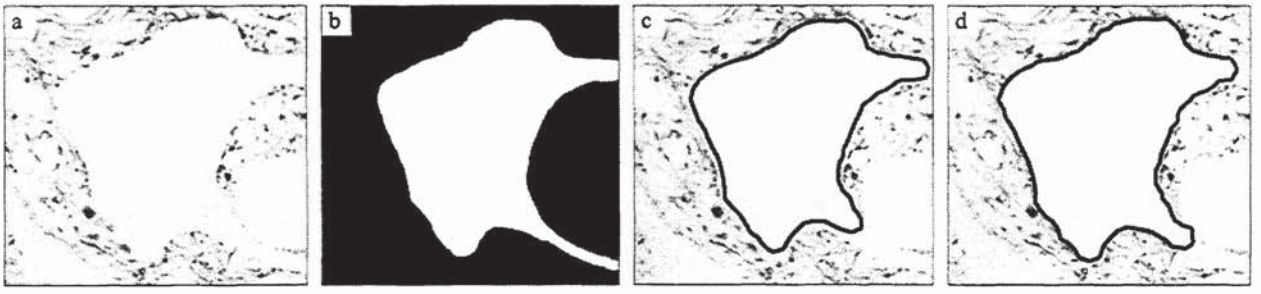

Figure 2. Segmentation of a histochemically stained motoneuron.

4.2. The Next Generation

The reproductive phase of the population starts by sorting the individuals according to their fitness function. The population $\{P_i\}$ evolves from generation to generation. A change consists of the following steps:

- From the current population, a fixed number of single–ancestor reproductions are selected. This random selection chooses parents with a Poisson–distribution so that individuals with higher fitness are more likely to become a parent.
- The single–ancestor reproduction creates a new child individual. The parameters of the child are randomly set with an equal distribution of the parameters in the range $[\mathrm{val}_{i,j} - \frac{1}{2}\mathrm{var}_{i,j}, \mathrm{val}_{i,j} + \frac{1}{2}\mathrm{var}_{i,j}]$. Randomly, in one fifth of all reproductions, the variability is multiplied with $\frac{5}{4}$ or $\frac{4}{5}$ to increase or decrease the variability of an evolving subpopulation.
- A fixed number of dual–ancestor reproductions are selected. Two parents are chosen according to the Poisson–distribution, the child's parameter set is first set to the mean of all values and variabilities and then changed with the rules described for the single–ancestor reproduction.

Following the reproductive phase, the age of all individuals in the population is incremented. Individuals that exceed a fixed maximum age are eliminated from the population. We did not define rules to detect the convergence of the population to an optimum, so far we use a fixed number of generations for the optimization of the parameter set by the genetic algorithm.

5. COLOR IMAGES

The formulation of external influences (Eq. 3) allows to process images with a value space W of higher dimension m. For these images, we first compute individual parameter sets for the image values w_c, which are components of $\vec{w}$, and define a quality Q_c for each channel c:

$$Q_c = \begin{cases} 0 & \forall \quad \widehat{E_c} \geq 0.25 \\ 25 - 100\widehat{E_c} & \forall \quad 0 \leq \widehat{E_c} < 0.25 \end{cases} \tag{15}$$

For a color segmentation, we combine the individual image potentials $\Phi_c(w_c)$ to form the vector $\vec{\Phi}(\vec{w})$, and synthesize $\vec{k}(h)$ from the filter kernels $\tilde{k}_c(h)$. These individual filter kernels were computed for each channel c and weighted according to their quality:

$$\tilde{k}_c(h) = k_c(h) \cdot \frac{Q_c}{\sum_{i=1}^{m} Q_i} \tag{16}$$

The strength s_d of the deformation force is likewise computed from the $s_{d,c}$ that are adjusted for each channel.

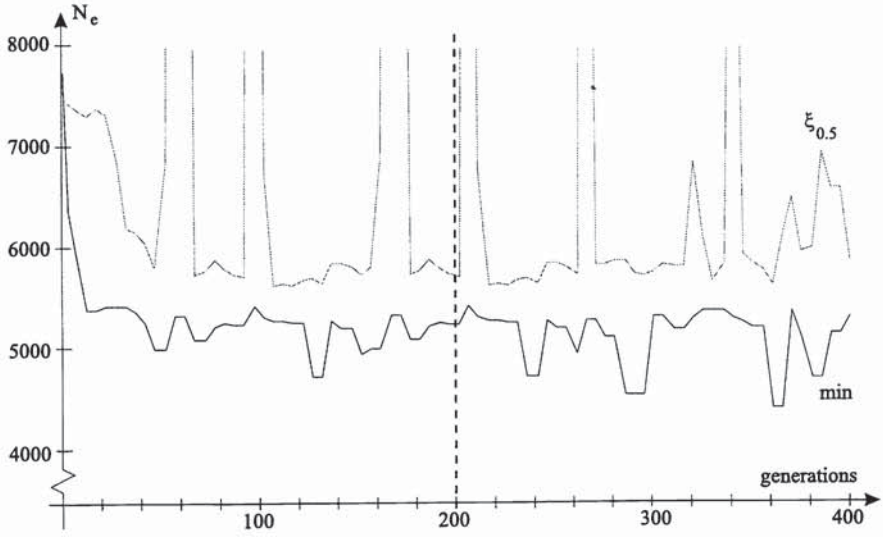

Figure 3. Minimum and median $\xi_{0.5}$ of N_e of a population during the genetic optimization of the parameter set. Usually, the algorithm ends after the 200^{th} generation.

6. RESULTS

The required manual segmentation can easily be drawn by physicians. Thereafter, the method operates automatically to adjust a parameter set from an exemplary original and its manual segmentation. For all medical images, we set $\Delta = 2$, $|p| = 2$, $S_p = 2$, and $\beta = 1$. The iteration ends if 95% of all vertices moved less than one pixel in the prior five iterations. The search for the optimal gradient ranges within $1 \leq d_1 < d_2 \leq 5$. The genetic algorithm runs for 200 generations. In every generation, five single–ancestor– and one dual–ancestor–reproductions take place, the maximal age of individuals is set to ten generations.

6.1. Assistance for Quantification of Similar Images

The deformable membrane model was already used for the detection of the neointima of vessels with implanted metal stents, to quantify morphological abberations of fibroblasts in contact with biomaterials, to document the resorption process of nets used as wound coverage, and the segmentation of histochemically stained motoneurons.[8] Parameter settings for these applications were now automatically computed. They result in the same detection quality as the parameter settings previously determined by manual interaction. The segmentation achieved before the optimization by the parameter set derived from one cell image (Fig. 2 a) and the manual segmentation (b) already yields the global shape of the cell (c). The genetic algorithm improves this result (d) and reduces N_e from 7730 down to 4751 pixel in 200 generations (Fig. 3). The major reduction of N_e takes place within the first 30 generations. The population does not converge into a stable optimum but remains active for the following hundreds of generations. Time and again, peaks in the curve of $\xi_{0.5}$ show the occurrence of subpopulations that do not give a segmentation result at all. Even though new best parameter sets are still found after the 200^{th} generation, no significant improvement takes place.

The remaining error is mainly caused by the axon that leaves the image in the lower right corner. The deformable membrane does not enter this narrow passage during the inflation process. Nevertheless, this segmentation error is irrelevant for the actual quantification task. This axon contains approximately 3500 pixel, the genetic algorithm reduces the average distance of the contour to the manual segmentation from 3.1 down to 0.89 pixel if this area is not considered. This parameter set was used to quantify a series of 137 motoneurons. All segmentations were visually inspected, the automatically detected contours were accepted for 127 cells (93%).

6.2. Segmentation of Color Images

As an example for a color segmentation, we apply the model to endoscopic images of the larynx. For phoniatric diagnoses, the vocal folds are captured under stroboscope light with a CCD–camera.[13] Segmentation only using

Table 1. Quality Q_c, classification error $\widehat{E_c}$ and resulting weight of external influences for different color spaces.

channel	$\widehat{E_c}$	Q_c	weight
red	31.6%	0	0
green	12.3%	12.7	0.53
blue	13.8%	11.2	0.47
hue	17.1%	7.9	0.39
saturation	12.8	12.2	0.61
value	24.5%	0.5	0
luminance	18.4%	6.6	0.23
u	15.0%	10.0	0.36
v	13.4%	11.6	0.41

greylevel information is not robust enough. The greylevel image results in $\widehat{E_c} = 24.5\%$ and, therefore, no segmentation result was found with the balloon model. Contrarily, a study in the color spaces RGB, HSV and LUV showed that the green and blue channel as well as hue and saturation and all channels in LUV color space give sufficient qualities $Q_c > 5$ (Tab. 1). The segmentation of images taken from clinical routine succeeds in all three image spaces for the combination of channels with $Q_c > 5$ (Fig. 4). The exact location of the detected boundary of the vocal folds varies. Further experiments are needed to decide which color space is superior for medical diagnostics.

7. DISCUSSION

The routine use of balloon models in medical image analysis was so far limited by the ability of physicians to adjust technical parameters. With our method, only a single manual segmentation is needed to adjust a balloon model to any specific segmentation tasks. Such methods are already used by different learning–by–example procedures.[3–5] Our method combines the advantages of analytic parameter computation with those of genetic algorithms and does not rely on propagation methods for the segmentation. Furthermore, it is applicable to color and other multi–channel images. Therefore, we are confident to intensify the use of these models in medical image processing.

It is recognized widely that the use of color information increases the potential power of image analysis. With our method, color channels can be evaluated for their applicability in medical image segmentation. It combines the individual properties of object's boundaries in different channels to one robust segmentation process.

For the segmentation of images stacks in spatial data or image sequences, we also test models that perform segmentations in three–dimensional space. The parameters that were adjusted for one image out of these stacks or sequences are applicable to a coherent segmentation in the entire data set.[7]

ACKNOWLEDGMENTS

The author holds a scholarship from the *Studienstiftung des Deutschen Volkes* (German Scholarship Foundation).

REFERENCES

1. T. McInerney and D. Terzopoulos, "Deformable models in medical image analysis: A survey," *Medical Image Analysis* **1**, pp. 91–108, 1996.
2. C. Xu and J. L. Prince, "Snakes, shapes, and gradient vector flow," *IEEE Transactions on Medical Imaging* **7**, pp. 359–369, March 1998.
3. S. Cagnoni, A. B. Dobrzeniecki, R. Poli, and J. C. Yanch, "Genetic algorithm–based interactive segmentation of 3D medical images," *Image and Vision Computing* **17**(12), pp. 881–895, 1999.
4. M. S. Horritt, "A statistical active contour model for SAR image segmentation," *Image and Vision Computing* **17**(3–4), pp. 213–224, 1999.
5. B. Levienaise-Obadia and A. Gee, "Adaptive segmentation of ultrasound images," *Image and Vision Computing* **17**(8), pp. 583–588, 1999.

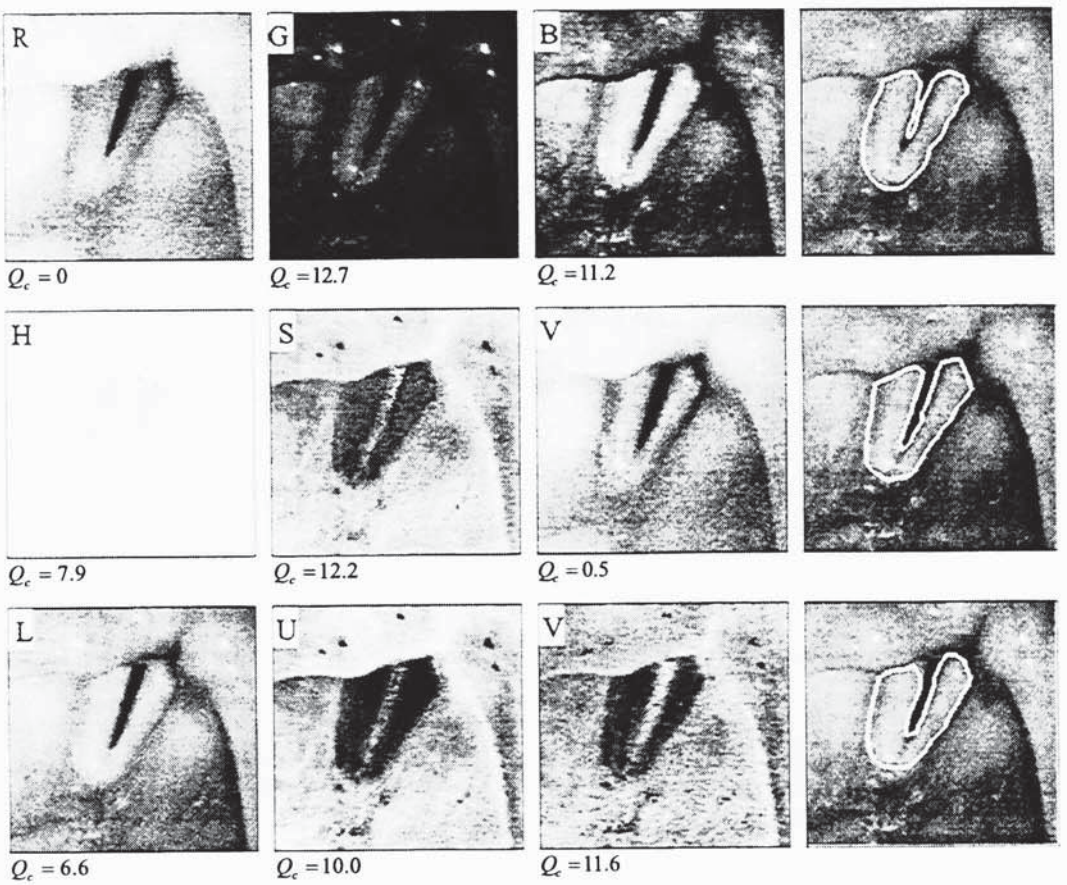

Figure 4. Laryngoscopic images in the color spaces RGB, HSV, and LUV, the respective segmentation result, and the quality Q_c for the different color channels.

6. L. D. Cohen and I. Cohen, "Finite–element methods for actice contour models and balloons for 2 D and 3 D images," *IEEE Transactions on Pattern Analysis and Machine Intelligence* **15**(11), pp. 1131–1147, 1993.
7. J. Bredno, T. Lehmann, and K. Spitzer, "A general finite element model for segmentation in 2, 3, and 4 dimensions," *Proc. SPIE* **3979**, 2000. (this issue).
8. V. Metzler, J. Bredno, T. Lehmann, and K. Spitzer, "A deformable membrane for the segmentation of cytological samples," *Proc. SPIE* **3338**, pp. 1246–1257, 1998.
9. T. Lehmann, C. Gönner, and K. Spitzer, "Survey: Interpolation methods in medical image processing," *IEEE Transactions on Medical Imaging* **18**(11), 1999. (in press).
10. K. Ngoi and J. Jia, "An active contour model for colour region extraction in natural scenes," *Image and Vision Computing* **17**(13), pp. 955–966, 1999.
11. C. Jordan, T. Ebrahimi, and M. Kunt, "Compression for retrieval of binary images," *Computer Vision and Image Understanding* **71**(2), pp. 198–212, 1998.
12. L. Davis, *Handbook of genetic algorithms*, Thomson Computer Press, London, 1996.
13. I. Scholl, A. Sovakar, T. Lehmann, and K. Spitzer, "Motion analysis of vocal folds using adaptive snakes," *Advances in Quantitative Laryngoscopy* **2**, pp. 29–38, (Erlangen–Nuremberg), 1997.